Calculation of Flow Along a Cowl of a Shrouded Propfan Using a 3D-Euler code

S.Leicher
Dornier GmbH, 7990 Friedrichshafen, FRG
P.Lücking and P.Wehlitz
MTU, 8000 München, FRG

Abstract

To support the aerodynamic design of the cowling of a counter-rotating integrated shrouded propfan (CRISP) 2D- and 3D-flow calculations have been performed. For the 2D-computations a computer program has been developed to analyse the axisymmetric flowfield through the rotors and over the cowling. To solve the 3D-Euler equations the well known Dornier 3D blockstructured flow analysis code was used. The grid generation which meets the special requirements for the CRISP configuration is described. The method generates a contour fitted grid meeting the demands of the finite volume flow solver. Because of the axisymmetric shape of the configuration an optimized section grid was built up first by use of a sigularity method, suitable stretching and shifting routines, a 2D-optimization method and a smoothing operator. Later the sectionwise grid was rotated and the total domain was devided into multiple topological rectangular blocks. The flow analysis method solves the 3D-Euler equations in arbitrarily blockstructured grids by a finite volume discretization technique and an explicit multi-stage time stepping scheme. The main advantage of the method is the applicability to complex geometries of nearly any shape, the capability to treat very fine grids with a theoretically unlimited number of grid points and rather fast convergence rates by means of incorporated multi-level and multigrid schemes.

Introduction

For the aerodynamic design of a counter-rotating shrouded propfan (CRISP) /1/ a computer program has been developed to analyse the axisymmetric flowfield of the connected flow through the rotors and over the cowling. The main purpose of this program is to design and to control the aerodynamics of the cowling profile. The cowling pressure distribution depends on the rotors and the hub contour and is subjected to large differences in the inflow conditions.

In addition to a low drag velocity distribution along the outer side of the cowling under cruise conditions, the flow should not separate at the critical operating points "take-off/initial climb" and "windmilling" (engine out). At take-off a high angle of attack is combined with a high fan mass flow with imminent flow separation from the inside of the lower cowling lip. A circumferential flow distortion at the fan entry increases the danger of fan flutter. At windmilling a separation of the flow from the outside of the upper cowling is possible due to the considerably reduced mass flow and the high angle of attack, which would lead to a strong drag rise of the nacelle.

A well established streamfunction method is used which meets the requirements of the calculation of a 2D-axisymmetric subsonic inviscid flow field; supersonic bubbles may occur locally and can be treated satisfactorily by a transonic approximation. The problem corresponds to the solution along a hub-to-tip streamsurface in a turbomachine which is often experienced in the field of quasi-3D flow calculations through cascades, e.g. /2/,/3/. The numerical solution is performed using finite differences. The mesh is generated numerically, and the resolution is finer near the leading edge to capture the strong flow gradients at the different flow conditions mentioned above.

For three-dimensional configurations there has been a considerable increase in the ability to compute connected flow fields. The level of the field equations which could be considered has increased from the small disturbance potential methods in the early seventies to full potential and Euler methods to today Navier-Stokes solutions. The complexity of the geometry which could be considered has also increased from singular components to more and more complicated complete configurations. Because of the great generality of the most commonly used finite volume technique the main difficulty in analyzing more complex configurations seems to be the grid generation for such complex geometries. So it can easily be seen, that the grid generation process becomes more and more important for the application of computational fluid dynamic problems.

In the current case of the axisymmetric CRISP configuration the block-structured grid technique is used /4/,/5/,/6/ and /7/ for the 3D-flow computations. The approach divides the computational domain into multiple topological rectangular blocks, which can be defined arbitrarily to produce surface-fitted grids. Such a subdivision of the physical space can be adapted to complex configurations with multi-components in such a way as to reduce grid skewness near the boundaries and provide good grid behaviour around the surface slope discontinuities. It undergoes also the storage restrictions of most of the today computers for fine 3D-grids because only one block has to be present in the main storage during the grid generation as well as during the flow solution,

The flow analysis method /8/,/9/ and /10/ solves the 3D-Euler equations using the numerical scheme developed by Jameson, Schmidt and Turkel /11/. This method is a central difference finite volume method combined with a second- and fourth-order dissipation. The steady state is reached by applying a Runge Kutta time stepping scheme with a variable number of stages. In order to accelerate convergence rates, local time stepping, enthalpy forcing and implicit residual averaging are used. By using a sequence of mesh refinements (multi-level grid technique) and applying a multigrid method /12/ at each of these levels, acceptable convergence rates for 3D-cases have been achieved. The method has been optimized with regard to computing time as well as to the amount of I/O which has to be performed. Also it has been extended to an arbitrary block structure, which allows the user nearly all freedom in the connection as well as in the arrangement of the blocks.

Very recently the code has been extented to solve the 3D-Navier-Stokes equations /13/ and a version which uses the benifits of parallising on virtual storage computers has also been implemented /14/.

The method has been applied to various external and internal flow problems with and without viscous effects /8/,/9/,/10/. Because the Euler equations are able to treat flow fields including vortices /9/. and variations of total pressure and total temperature, they can be applied very easily to cases including propulsion effects on aerodynamic components or complete configurations.

Axisymmetric Streamfunction Method

Description of Method

A meridional flowfield is calculated along a single meridional (hub-to-tip) streamsurface which may be regarded as part of a 3D-solution where several 2D-calculations along meridional and circumferential streamsurfaces are used iteratively /3/,/15/. The partial solutions on the surfaces are 2D when the kinematic condition -the flow must follow a given surface- is satisfied. The prescription of a swirl distribution is equivalent, and is used here. The solution along the single streamsurface surface is regarded as axisymmetric.

A streamfunction is defined by the continuity equation and then introduced into the radial component of the inviscid equation of motion, which leads to a second order partial differential equation for the streamfunction along a meridional streamsurface. The type of the equation is elliptic for a meridional Mach number below unity. For the purpose of the numerical solution, using finite differences, the flowfield is covered with a contour-fitted mesh. The coordinates of the grid points themselves are numerical solution of a system of Poisson equations according to Thompson et al./16/,/18/. A coordinate transformation is performed using the grid lines as coordinate lines, so that the differentials can easily be discretized by the usual central second order approximations. The resulting systems of algebraic equations for the streamfunction or for the mesh coordinates are solved iteratively by successive overrelaxation.

The streamfunction equation is non-linear because the coefficients depend on the solution. The coefficients are found iteratively during the computation and can be determined from the density. The density is derived from the streamfunction field with the help of the total enthalpy calculated from the prescribed swirl and the angular velocity of the rotors. Especially for transonic flowfields the use of mass-flow density (differential of streamfunction) is not unique and also the dependence of the density is indefinite. Here the radial component of the equation of motion is solved directly to determine the velocity.

The boundary conditions for the stream- function calculation are a homogeneous fully prescribed inflow, an axial outflow, a farfield condition along the outer radius of the solution domain, and the contour condition of constant streamfunction along the hub and the cowling. The cowling trailing streamline is a discontinuity line (slip line) in the case where work is done by the rotors. It separates two regions of different total state but continuous static pressure. The streamfunction differentials are not continuous so that no solution is possible across that line. The cowling trailing grid line is regarded as a slip line and should have the streamfunction value of the cowling contour. During the course of the iterative solution it is fitted to the right position of the trailing streamline. Under the condition of equal static pressure on both sides of the slip line there exists a relation for the streamfunction value at a slipline grid point (boundary condition). The value at the cowling trailing edge is valid on the whole contour (Kutta condition). During the iterative solution new trailing streamlines are interpolated with this value from the calculated streamfunction distribution, so that the mesh can be fitted accordingly and converges with the solution

Results of Computation

To calculate the meridional flowfield of a counter rotating shrouded propfan a numerically generated mesh is used, as represented in Fig. 1.1 . The drawing demonstrates the extension of the solution domain. The detail in Fig. 1.2 shows the fine resolution of the mesh near the cowling, especially near the leading edge. The profile of the rotors can be recognized as gridlines.

A streamfunction computation has been performed on this grid for the propfan under max climb conditions at zero angle of attack and at a freestream Mach number of 0.8. The change of swirl through the rotors and their blockage effect are prescribed from a design calculation. The fan mass flow depends on the specific rotor work (change of swirl and angular rotor velocity) and on the Kutta condition at the cowling trailing edge, and results from the calculation. The computed Mach number field is shown in Fig. 1.3 for the rotor and cowling section. Fig. 1.4 illustrates the calculated shroud Mach number distribution over the cowling.

Measurements of the pressure distribution over the cowling of a turbine propulsion simulator (TPS) have been performed at the DFVLR /17/. To compare them with calculated results the cowling profile has been taken separately with some simplification in the rotor region. In Fig 1.5 a detail of the mesh is drawn together with the true TPS geometry. A calculation has been carried out without rotor work but with a given measured mass flow. The cowling trailing gridline has been fixed and treated as a solid wall. Fig. 1.6 shows the calculated profile Mach number distribution, and the measured values are added for comparison.

3D-Euler Calculations

Grid Generation

The blockstructured grid used within these computations is generated in a somewhat different way compared with to the procedures described in /5/,/7/. Because the configuration possesses axial symmetry the grid generation is done in two steps. First a 2D-section grid was calculated, which in the second step was rotated.

Before generating the sectionwise grid the overall blockstructure is designed as shown in Fig. 2.1. The total grid exists out of six blocks in i-direction while the j- and the circumferrential k-direction is kept unblocked. The blocks are arranged in such a way that each blockface as only one unique boundary condition.

Starting point for the grid generation is a singularity method with singularities placed in the nose of the center body and the cowl. The exact location can be prescribed by input to influence the behaviour of the grid lines in the vicinity around the noses parts to get gridlines nearly orthogonal to the contour.

Using such a singularity method, there is no direct influence upon the final point distribution throughout the total domain. Therefore we use the following subsequent steps to get an improved mesh which also meets the requirements of a multi-level as well as a multigrid technique:

Prescribe and limit the outer farfield boundary.

Prescribe the behaviour of the wake of the cowl to avoid cells with high aspect ratios near the upstream farfield.

Shift the i-lines in such a way that the i-index at the block boundaries meets the requirements of a multigrid method.

Revise the point distribution in j-direction to increase the grid density at the body surfaces.

Optimize the grid generated so far by applying a 2D-optimization method and/or an smoothing operator.

The optimization method used comprises the solution of a partial differential equations of the form (here for 3D) of a Poisson equation /16/,/18/:

$$\xi_{xx} + \xi_{yy} + \xi_{zz} = P(\xi,\eta,z) \tag{1}$$

$$\eta_{xx} + \eta_{yy} + \eta_{zz} = Q(\xi,\eta,z)$$

$$z_{xx} + z_{yy} + z_{zz} = R(\xi,\eta,z)$$

where (ξ,η,z) are the computational, and (x,y,z) the physical coordinates. P, Q and R are source terms which control the interiour grid spacing. The above equations can be transformed to the computational coordinates (ξ,η,z) by interchanging the role of dependent and independent variables. This leads to a quasi-linear elliptic system of equations:

$$A X_{\xi\xi} + B X_{\eta\eta} + C X_{\zeta\zeta} + D X_{\xi} + E X_{\eta} + F X_{\zeta} = 0 \tag{2}$$

wherein the X = (x,y,z) are the cartesian coordinates of the grid points. These equations are solved for specified regions of the domain by succesive line over relaxation (SLOR). The coefficients A to F are constant or specified functions used for grid control. The grid control terms are defined along each block boundary and then interpolated across the interior grid. At the boundaries, the values are estimated by the condition, that all derivatives normal to the boundary in equation (1) vanish.

Across the boundaries of such a grid block a suitable smoothing operator was applied to avoid kinks in the behaviour of the gridlines.

The final section grid can be seen in Fig. 2.2. IT has at least two features which schould be mentioned. One is that special care has been taken to design the grid in the nose region of the center body. The other point is the increased grid density at the location of the actuator disk and the fact that the i-lines became here also (x = const.)-lines (Fig. 2.3). The actuator disk plane is designed to be an internal boundary and has also to match the multigrid requirements. It has been placed in the midplane between both propellers. Fig. 2.4 shows a view of the total surface grid while Fig. 2.5 represents a crossection at the location of the propfan. The increased grid density towards the surfaces can be seen quite clearly.

After the final step of rotating the total grid is separated in i-direction into the six blocks according to the designed block structure.

Flow Analysis Method

Governing Equations

The Euler equations describing three-dimensional, unsteady and compressible flows in conservation form read

$$\frac{\partial U}{\partial t} + \frac{\partial F1}{\partial x} + \frac{\partial F2}{\partial y} + \frac{\partial F3}{\partial z} = 0 \tag{3}$$

where:

$$U = \begin{bmatrix} \rho \\ \rho u \\ \rho v \\ \rho w \\ E \end{bmatrix} \tag{4}$$

$$F1 = \begin{bmatrix} \rho u \\ \rho u^2 + p \\ \rho uv \\ \rho uw \\ (E+p)u \end{bmatrix}, \quad F2 = \begin{bmatrix} \rho v \\ \rho uv \\ \rho v^2 + p \\ \rho vw \\ (E+p)v \end{bmatrix}, \quad F3 = \begin{bmatrix} \rho w \\ \rho uw \\ \rho vw \\ \rho w^2 + p \\ (E+p)w \end{bmatrix}$$

with density ρ and mean total energy per unit volume E:

$$E = \rho e + 0.5(u^2 + v^2 + w^2) \tag{5}$$

The perfect gas equation of state is used to define the mean pressure p via the internal energy e:

$$p = (\gamma - 1)\rho e \tag{6}$$

Finite Volume Method

Applying equation (3) integrated in space to each cell of the computational domain separately where all physical properties are defined to be constant the resulting system of ordinary differential equations are solved in time by the following explicit 3-stage Runge-Kutta-like multi-stage method /11/.

$$\begin{aligned} u^{(0)} &= u^n \\ u^{(1)} &= u^{(0)} - \alpha_1 P u^{(0)} \\ u^{(2)} &= u^{(0)} - \alpha_2 P u^{(1)} \\ u^{(3)} &= u^{(0)} - \alpha_3 P u^{(2)} \\ u^{n+1} &= u^{(3)} \end{aligned} \tag{7}$$

where n denotes the previous time-level and P represents a spatial central difference operator. Due to its effectiveness as well as to robustness the 3-stage scheme (7) has been applied for all calculations. According to the need to damp out high frequency error during the multigrid cycle the following coefficients are used.

$$\alpha_1 = 0.60 \qquad \alpha_2 = 0.60 \qquad \alpha_3 = 1.00 \tag{8}$$

Filtering Techniques

To prevent an odd-even decoupling, blended second and fourth order artificial dissipation /11/ is used. If the filtering technique is applied only once, stability analysis indicates the best damping property as well as the largest extension of the stability region to the left of the real axis giving freedom in the introduction of dissipative terms. In practice, the fourth order filter is active throughout the computational domain providing a back ground damping except in areas with larger pressure gradients where the second order filter is switched on. Special filter formulations at solid walls minimize the numerical error. Across block faces it is insured that the construction of the filter terms across these boundaries are the same as inside each block. An special filter function has been applied in the nose part of the center body decreasing the influence of the 4th-order term to zero for the i- and j-direction while approaching this particular point.

Block Logic
The newest version of the flow solver is very flexible with regard to the block logic. The different blocks may be distributed arbitrarily and arranged in the way of a linear graph. Only the neighbouring blocks which border on the current block and/or the kind of boundary condition have to be known. These is done by a five digit integer input variable. Several further improvements have been coded in the meantime. Across internal block boundaries index range refinements as well as coarsenings are allowed today and segmentations are possible. In principle the solution sequence is prescribed by the place of each block within the linear graph but there is also the possibility to solve blocks only every second or third cycle (for blocks near the farfield) or to solve some other blocks for example twice or even more during each cycle. Also it may be possible to solve different equations inside each block. It seams to make no sense to solve for example the 3D Navier-Stokes equations throughout the total computational domain while viscous effects are only concentrated around the geometry and in wake or mixing regions.

Boundary Conditions
As mentioned above the boundary conditions for each block face must be known. Internal block interfaces are treated as in an unblocked domain. At the solid walls boundary no-flux conditions are used combined with a pressure extrapolation to the wall. The farfield conditions are based on the introduction of Riemann invariants /9/ for a one-dimensional flow normal through the boundary. For supersonic flow however, all values are fixed for incoming flow and linear extrapolation are used for outgoing flow.

Beneath this standard conditions a lot of others have been incorporated such like:

Inflow and outflow conditions for internal or combined internal external problems.

Actuator disk conditions for cases with propellers, propfans or jets (see next part).

Special conditions for singular lines or points if one block face has such an irregular shape.

A condition to connect block faces by itself in C-type grids for example.

Propeller Simulation
The propeller is simulated by introducing an actuator disk along a computational mesh plane as proposed by /8/. Both tractor as well as pusher types can be treated by the current version of the code. Because of the C-type mesh used the disk is represented by a number of rectangular cells and is not a real circle. If the distribution of the total pressure p_t, the total temperature T_t and the swirl angle δ is known upstream of the disk the problem can be solved as follows:

Extrapolate the velocity q_2 from downstream. Calculate the Mach number M_2 by use of q_2 and the total temperature T_t (dimensionless quantity as usual).

$$M_2^2 = q_2^2/(\gamma T_{t2} - 0.2q_2^2) \tag{7}$$

The static pressure p_2 can be obtained from M_2 and p_t through the isentropic relation.

$$p_2 = P_t/(1. + 0.2M_2^2)^{3.5} \tag{8}$$

In connection with the known swirl angle δ the velocity components u_2, v_2, and w_2 can be computed. Finally the density ρ_2 is calculated by the definition of the total enthalpy H_t. The continuity across the disk i.e. the normal mass flux ρq_n is used as boundary condition for the upstream part of the disk.

Using this approach a problem arises with combining propeller simulation and Navier-Stokes calculations where total pressure losses are present in the boundary layer and in separated flow regions. It is obvious that a propulsion system changes the local flow properties instead of fixing an absolute level. So the total pressure p_t is rather calculated by adding a prescribed delta p_t to the local value in front of the disk. The same problem may occur in a weaker form during Euler calculations if total pressure losses or gains are derived.

Acceleration Techniques

Introducing the residual averaging approach /11/, i.e. collecting the information from residuals implicitly, permits stable calculations beyond the ordinary Courant number limit and accelarates convergence. Other acceleration techniques are the enthalpy forcing, the use of the local allowed maximum time step and at last a multigrid method. Because of the actuator disk boundary condition the enthalpy forcing idea can not be used. Throughout all calculations three grid levels are used with at least three multigrid levels in the finest grid.

Results

Two selected cases have been studied both being special design points. The first is the maximum climb at M = 0.8 Alpha = 0.0 degrees and the other is the most critical takeoff case at M = 0.25 Alpha = 24 degree. The ratios of the total pressure across the actuator disk is shown in Fig. 2.6. For the increase in total temperature a isentropic efficiency of η = .9 is assumed. Because the propfan syste comprises two counter-rotating propellers no swirl angle δ has to be considered.

The 3D-Euler calculations are performed to see the transonic effects and to get information about the three dimensionality of the flow. These problems have not or only insufficiently been resolved by the streamline method used in the design process.

Maximum Climb Case
In the maximum cruise case at M = 0.8 and α = 0.0 degree the question is if high supersonic Mach numbers may occur anywhere in the flow field. Fig. 2.7 shows the cp, the Mach number and the total pressure behaviour around the cowling and the centerbody. Because this case is a symmetric one only the upper part of the flowfield is presented. The work of the fan can be seen quite clear by the 25% increase in total pressure. Because the cp-value is normalised with p sub infinity it is positive behind the disk although the flow is accelerated. The Mach number distribution shows a supersonic flow region at the inner side of the cowl just behind the nose caused by the shape of cowl surface. After a small subsonic part the flow accelerates to supersonic again towards the actuator disk. Through the disk and behind the flow is subsonic because the local speed of sound is increased by the total temperature change. The acceleration at the center body is quite continous. A line plot around the surface makes the situation more clear (Fig. 2.8).

Takeoff Case
The takeoff calculations at M = 0.25 and α = 24.0 degree is a rather critical case. As Fig. 2.9 shows is there a region of high total pressure losses at the inner side of the lower part of the cowl. This losses originate from the nose as Fig. 2.10 illustrates where Mach numbers up to 1.8 are achieved at the leading edge. Because of the high angle of

attack the stagnation points is located relatively far away from the nose at the outside of the cowl (Fig. 2.11). The acceleration of the flow around the now " wrong shaped " cowl geometry leads to such a high machnumber peak. The total pressure losses on the other side lead to flow separation in the region of deceleration in front of the disk as Fig. 2.10 also indicates. Fig. 2.12 shows the machnumber distribution for the mid plane.

The 3D-Euler calculations show, that it is necessary to modify the cowling contour in the nose region to guarantee undisturbed operation of the rotors for the most critical operation points where especially in the takeoff case non satisfactory results have been obtained.

Conclusion

A 2-d streamfunction method for axisymmetric flowfields and a 3D-Euler method have been successfully used to support the design of an counter-rotating shrouded propfan (CRISP). The computational results for some critical flow conditions have been presented. They stress the capabilities of both methods.

It has been shown that the Dornier blockstructured 3D-Euler method is capable to solve three-dimensional flow problems with incorporated propulsion systems and that it is very flexible in the applicability.

References

1. *R. LINDLAUF, D. ECKARDT, L. BATTEZZATTO*
Advanced Technologies for New Generation Ducted Engines,AIAA/ASME Propulsion Conference, 1987.

2. *C. H. WU*
a General Theory of Three-Dimensional Flow in Subsonic and Supersonic Turbomachines of Axial, Radial , and Mixed-Flow Types, Trans. ASME , 1952.

3. *P. LÜCKING*
Numerische Berechnung von axialsymmetrischen Propfan-Strömungsfeldern mit einem Stromfunktionsverfahren, MTU Technischer Bericht 011-88, 1988.

4. *N. J. Yu*
Grid Generation and Transonic Flow Calculations for Wing-Body Combinations. Boeing Report D6-45277/1980, 1980

5. *K. D. Lee*
3-D Transonic Flow Computations Using a Grid System with Block Structure. AIAA paper 81-0998, 1981

6. *S. Leicher, W. Fritz, J. Grashof, J. Longo*
Mesh Generation Strategies for CFD on Complex Configurations. Paper in Lecture Notes in Physics Vol.170 Springer Verlag 1982

7. *W. Fritz*
Numerical Grid Generation around Complete Aircraft Configurations. AGARD, 58th Meeting on Aplications of Computational Fluid Dynamics in Aeronautics, 7-10 April 1986, AIX-EN-PROVENCE, FRANCE

8. *S.Leicher*
Numerical Simulatiom of Internal and External Inviscid and Viscous 3-D Flow Fields. AGARD, 58th Meeting on Aplications of Computational Fluid Dynamics in Aeronautics, 7-10 April 1986, AIX-EN-PROVENCE, FRANCE

9. *S. Leicher*
Analysis of Transonic and Supersonic Flows around Wing-Body-Combinations. ICAS 84-1.2.2, 1984.

10. *S. Leicher*
Numerical <solution of 3-D Invisid Flow Fields around Complete Aircraft Configurations. ICAS 86-1.3.2, 1986.

11. *A. Jameson, W. Schmidt, E. Turkel*
Numerical Solutions for the Euler Equations by Finite Volume Methods Using Runge Kutta Time Stepping Schemes. AIAA Paper 81-1259, 1981.

12. *A. Jameson, T. J. Baker*
Multigrid Solution of the Euler Equations for Aircraft Configurations. AIAA Paper 84-0093, Jan. 1984.

13. *S. Leicher, H. Rieger*
Computation of Some Turbulent Complex 3-D Flows in the Low Speed and High Speed Range. AGARD, Symposium on Fluid Dynamics of 3-D Turbulent Shear Flows and Transition, 3-6 October 1988, Cesme, Turkey

14. *S. Leicher*
Parallel Processing on Virtuell Storage Multiprocessor systems in CFD Simulation Employing Domain Splitting Techniques. IBM Symposium, August 1986, Oberlech, Austria

15. *P. LÜCKING*
Numerische Berechnung von axialsymmetrischen Propfan-Strömungsfeldern mit einem Stromfunktionsverfahren, MTU Technischer Bericht 011-88, 1988.

16. *J. F. THOMPSON, F. C. THAMES, C. W. MASTIN*
Boundary-Fitted Curvilinear Coordinate Systems for Solution of Partial Differential Equations on Fields Containing Any Number of Arbitrary Two-Dimensional Bodies, NASA-CR-2729, 1977.

17. *R. KIOCK, W. STAEGER*
Druckverteilungsmessungen an einem Modelltriebwerk bei inkompressibler Windkanalströmung, DFVLR-IB-129-87/39, 1987.

18. *J. F. Thompson*
Grid Generation Techniques in Computational Fluid Dynamics. 1983 AIAA Paper 83-0447

Figures

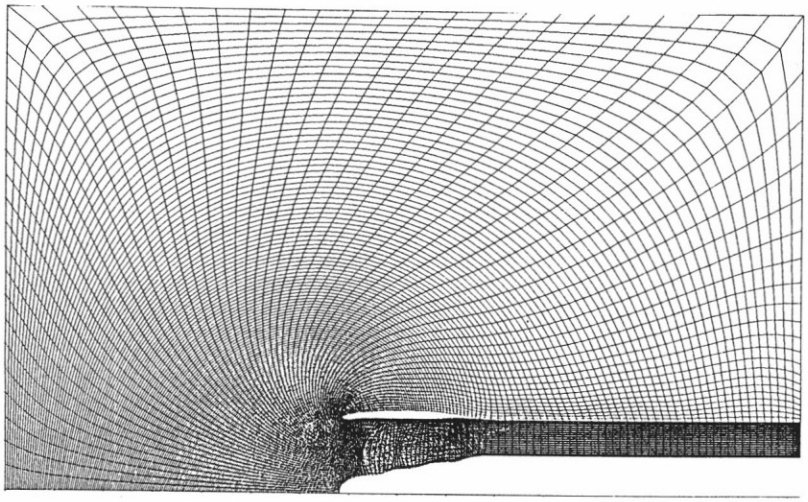

FIGURE 1.1. Calculation grid for a CRISP-configuration

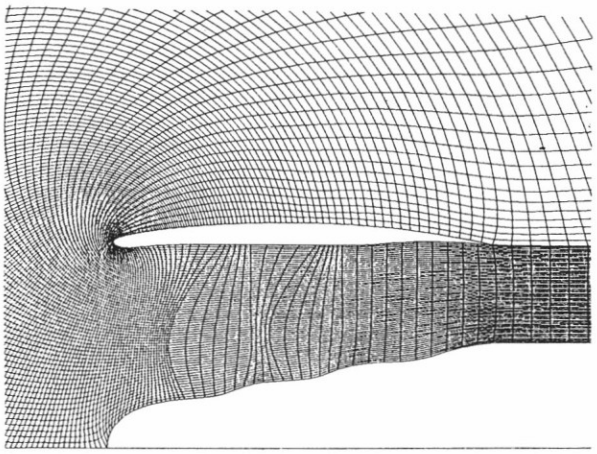

FIGURE 1.2. Grid detail from figure 1.1

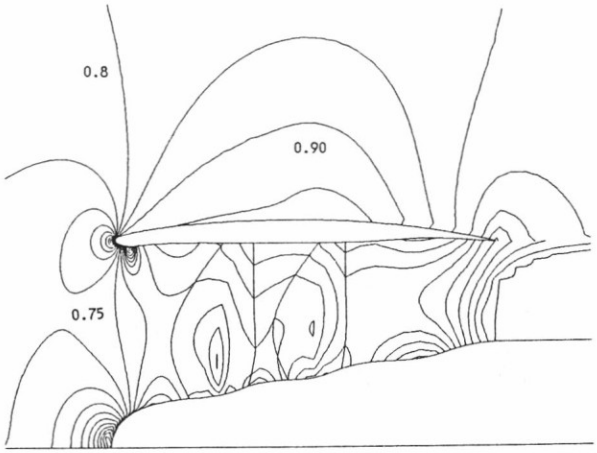

FIGURE 1.3. Detail of calculated Mach number distribution

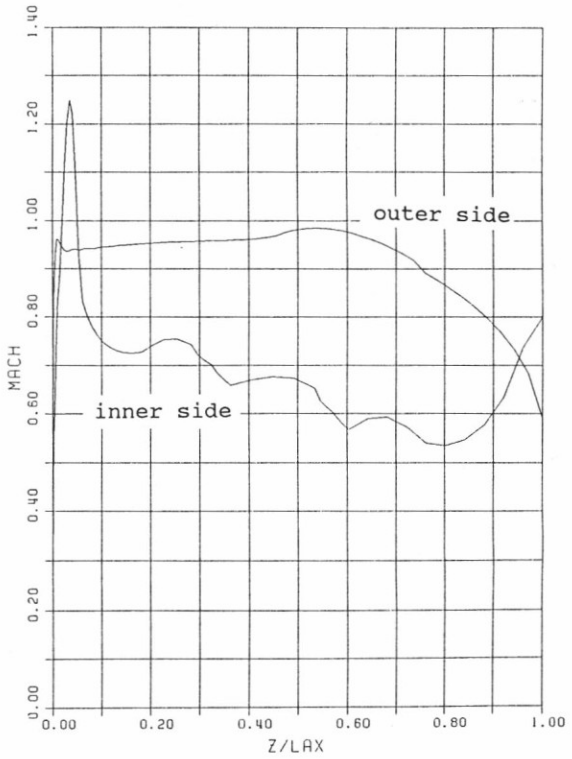

FIGURE 1.4. Calculated Mach number along cowling contour

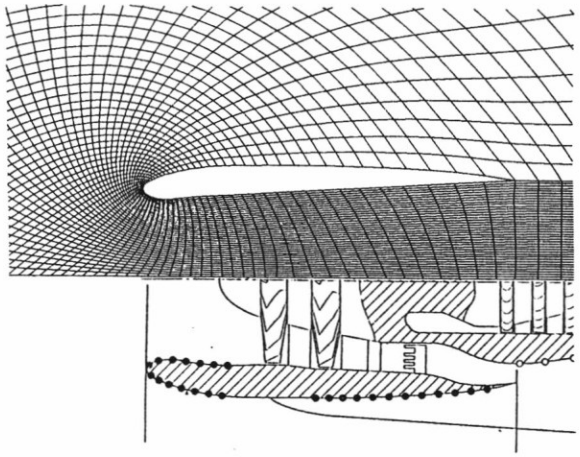

FIGURE 1.5. Configuration of a Turbine Propulsion Simulator and grid detail

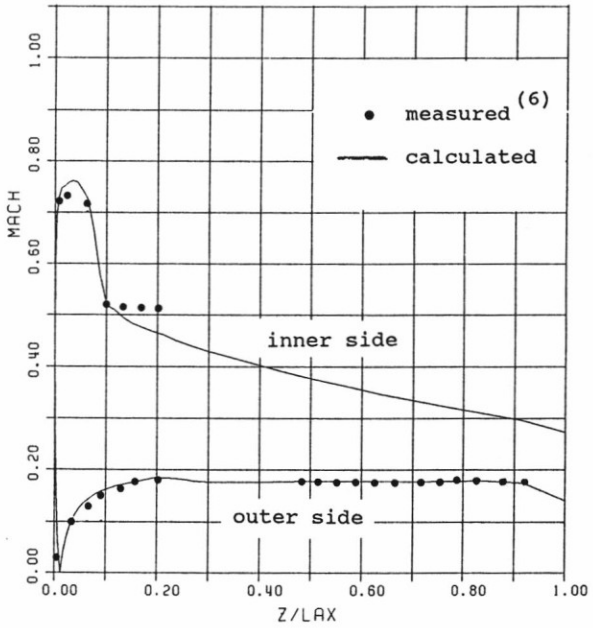

FIGURE 1.6. Comparison of measured and calculated profile Mach number distribution

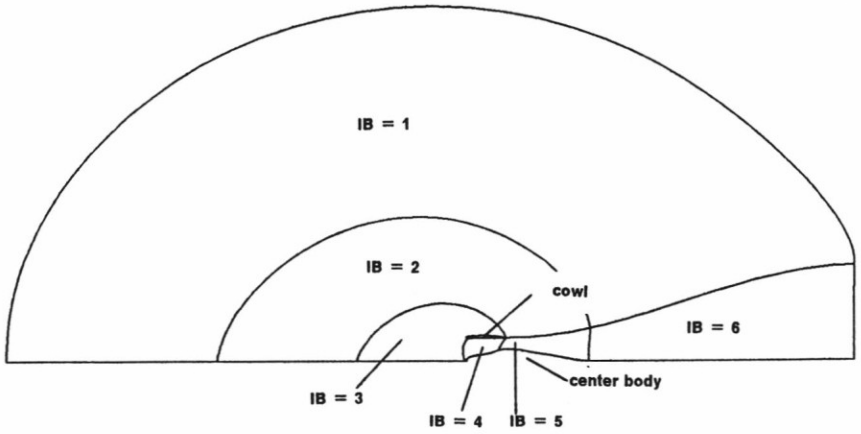

Fig. 2.1: ***Blockstructure for the CRISP Configuration***

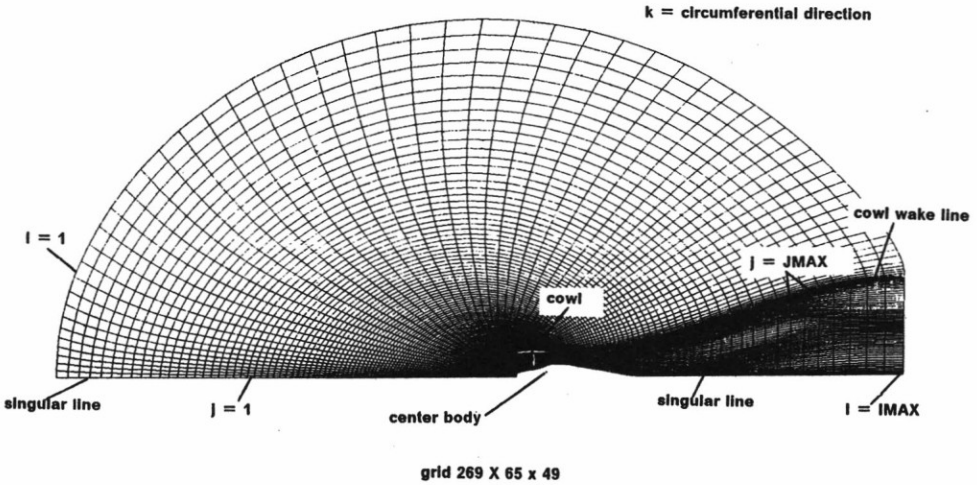

Fig. 2.2: ***Sectionwise Grid***

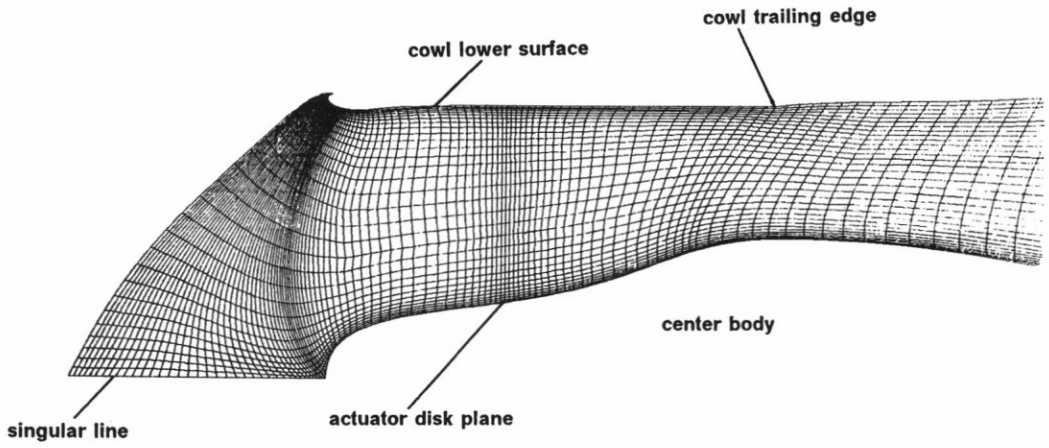

Fig. 2.3: ***Actuator Disk Region***

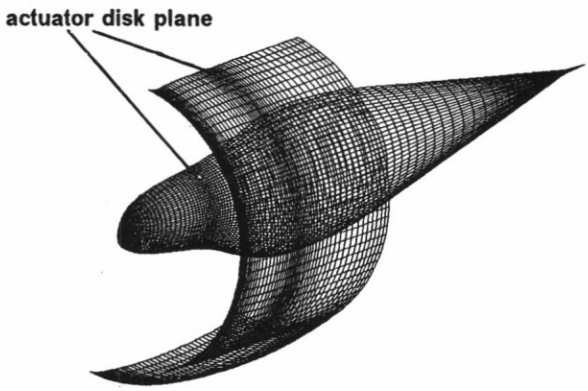

Fig. 2.4: ***Surface GRID***

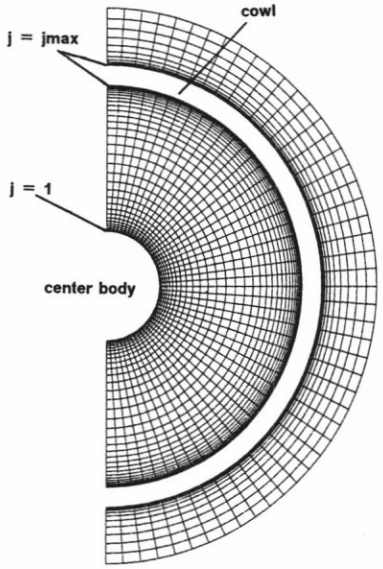

Fig. 2.5: ***Grid in a Crossplane***

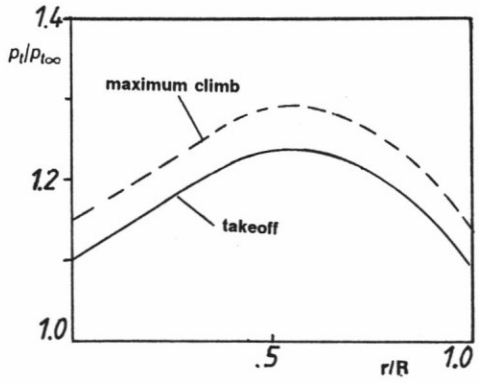

Fig. 2.6: ***Ratio of Total Pressures across Actuator Disk***

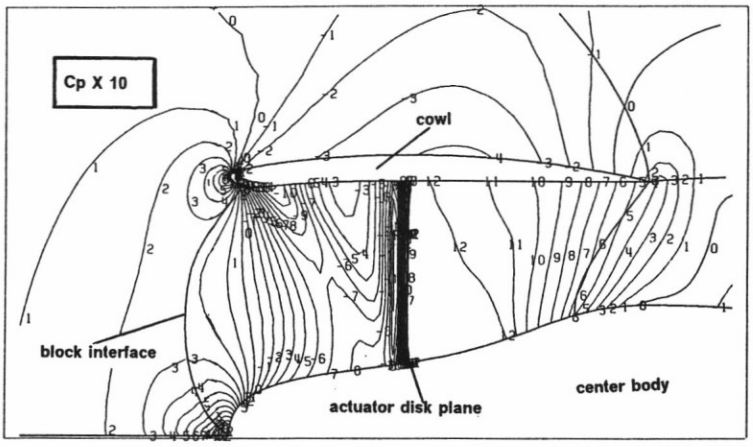

Fig. 2.7.a: ***Cp-Distribution (M = 0.8 Alpha = 0.0)***

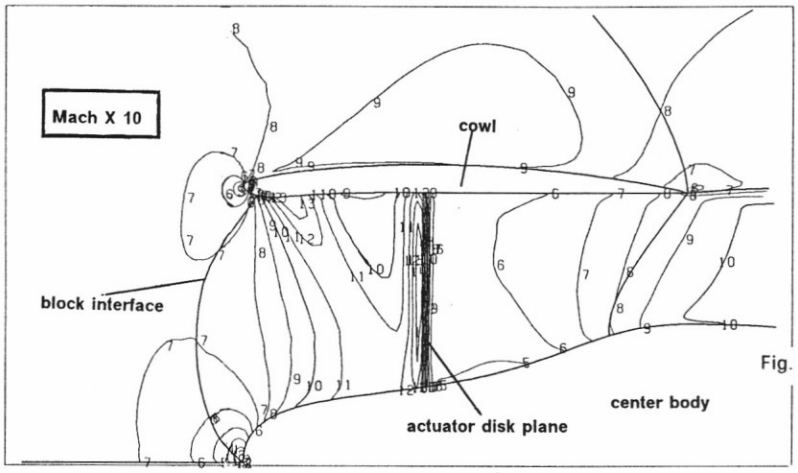

Fig. 2.7.b: ***Iso-Machlines (M = 0.8 Alpha = 0.0)***

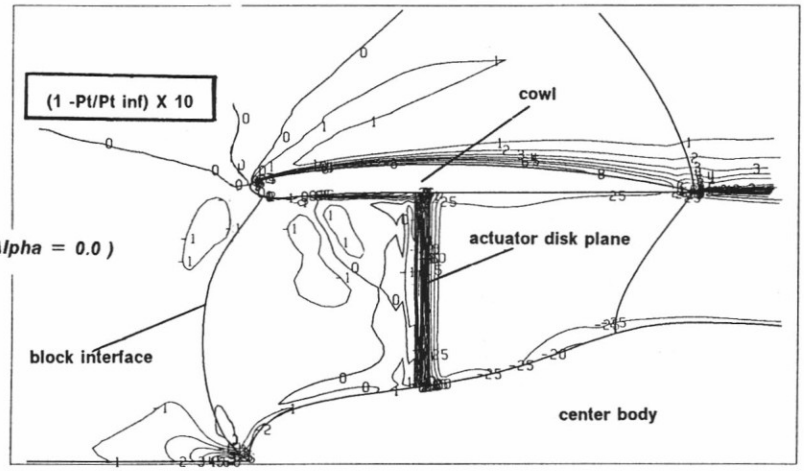

Fig. 2.7.c: ***Total Pressure Losses (M = 0.8 Alpha = 0.0)***

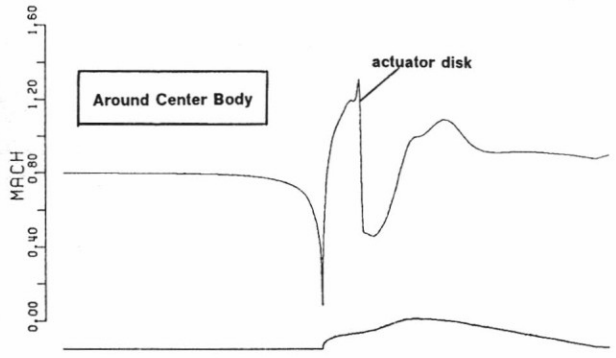

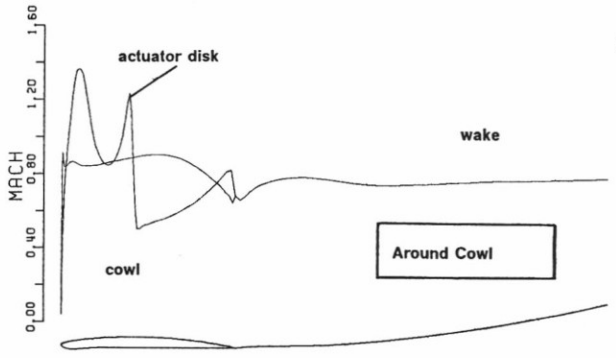

Fig. 2.8: ***Machnumber around the Contour of Cowl and Center Body***

(M = 0.8 Alpha = 0.0)

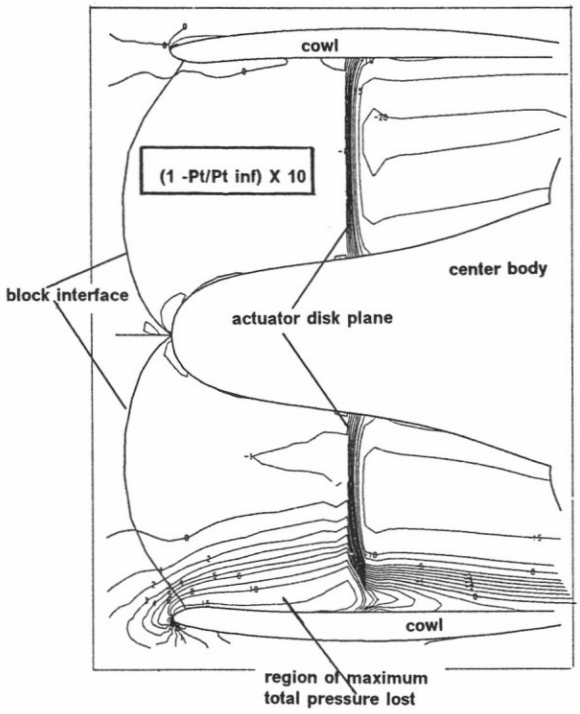

Fig. 2.9: ***Total Pressure Losses (M = 0.25 Alpha = 24.0)***

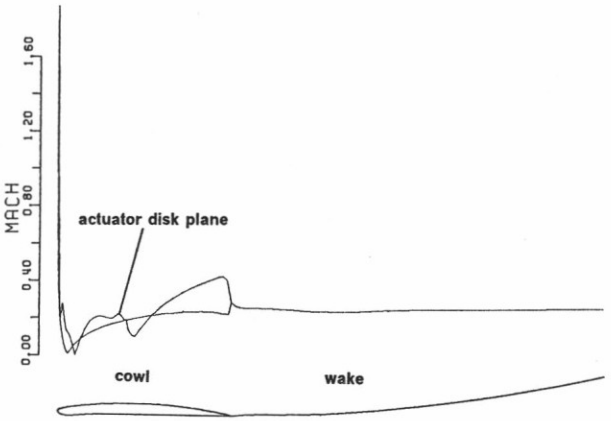

Fig. 2.10: ***Machnumber Distribution (M = 0.25 Alpha = 24.0)***

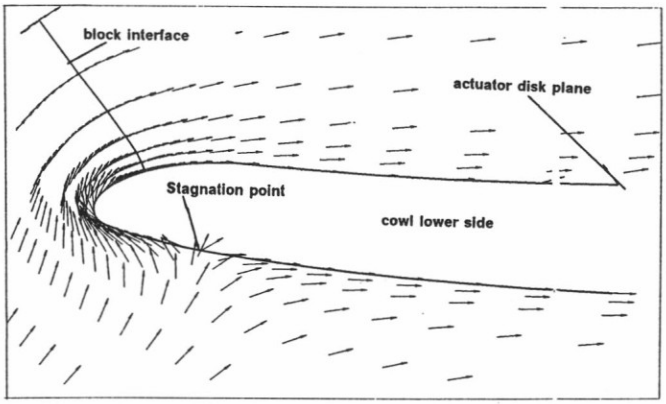

Fig. 2.11: ***Velocity Vectors (M = 0.25 Alpha = 24.0)***

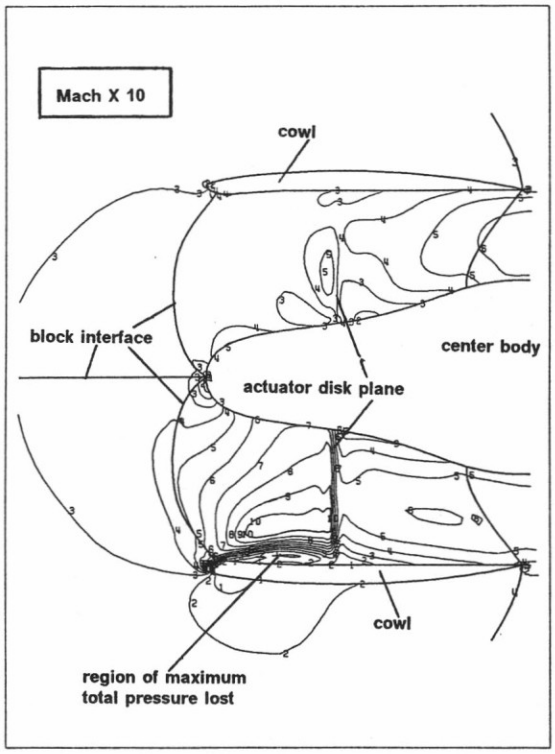

Fig. 2.12: ***Iso-Machlines (M = 0.25 Alpha = 24.0)***